Light harvesting enhancement in solar cells with quasicrystalline plasmonic structures

Christina Bauer* **and Harald Giessen**

4th Physics Institute and Research Center SCoPE, University of Stuttgart, 70550 Stuttgart, Germany
**c.bauer@pi4.uni-stuttgart.de*

Abstract: Solar cells are important in the area of renewable energies. Since it is expensive to produce solar-grade silicon [Electrochem. Soc. Interface **17**, 30 (2008)], especially thin-film solar cells are interesting. However, the efficiency of such solar cells is low. Therefore, it is important to increase the efficiency. The group of Polman has shown that a periodic arrangement of metal particles is able to enhance the absorbance of light [Nano Lett. **11**, 1760 (2011)]. However, a quasicrystalline arrangement of the metal particles is expected to enhance the light absorbance independent of the incident polar and azimuthal angles due to the more isotropic photonic bandstructure. In this paper, we compare the absorption enhancement of a quasiperiodic photonic crystal to that of a periodic photonic crystal. We indeed find that the absorption enhancement for the quasicrystalline arrangement shows such an isotropic behavior. This implies that the absorption efficiency of the solar cell is relatively constant during the course of the day as well as the year. This is particularly important with respect to power distribution, power storage requirements, and the stability of the electric grid upon massive use of renewable energy.

OCIS codes: (050.5298) Photonic crystals; (250.5403) Plasmonics; (310.6860) Thin films, optical properties; (350.6050) Solar energy.

References and links

1. A. Verbruggen and V. Lauber, "Basic concepts for designing renewable electricity support aiming at a fullscale transition by 2050," Energy Policy **37**(12), 5732–5743 (2009).
2. D. Fertl, "Germany: Nuclear power to be phased out by 2022," *http://www.greenleft.org.au/node/47834* (2011). Accessed: 23/08/2012.
3. F. Trieb, "Trans-mediterranean interconnection for concentrating solar power," Study report, German Aerospace Center (2006).
4. M. Tao, "Inorganic photovoltaic solar cells: Silicon and beyond," Electrochem. Soc. Interface **17**, 30–35 (2008).
5. D. Redfield, "Multiple-pass thin-film silicon solar cell," Appl. Phys. Lett. **25**(11), 647–648 (1974).
6. J. Zhao and M. A. Green, "Optimized antireflection coatings for high-efficiency silicon solar cells," IEEE Trans. Electron. Dev. **38**(8), 1925–1934 (1991).
7. B. O'Regan and M. Grätzel, "A low cost, high-efficiency solar cell based on dye-sensitized colloidal TiO_2 films," Nature **353**(6346), 737–740 (1991).
8. M. Grätzel, "Dye-sensitized solar cells," J. Photochem. Photobiol. C **4**(2), 145–153 (2003).
9. J. C. Goldschmidt, M. Peters, A. Bösch, H. Helmers, F. Dimroth, S. W. Glunz, and G. Willeke, "Increasing the efficiency of fluorescent concentrator systems," Sol. Energy Mater. Sol. Cells **93**(2), 176–182 (2009).
10. S. E. Han and G. Chen, "Optical absorption enhancement in silicon nanohole arrays for solar photovoltaics," Nano Lett. **10**(3), 1012–1015 (2010).
11. C. Haase and H. Stiebig, "Optical properties of thin-film silicon solar cells with grating couplers," Prog. Photovolt. Res. Appl. **14**(7), 629–641 (2006).
12. H. R. Stuart and D. G. Hall, "Absorption enhancement in silicon-on-insulator waveguides using metal island films," Appl. Phys. Lett. **69**(16), 2327–2329 (1996).
13. V. E. Ferry, M. A. Verschuuren, H. B. T. Li, R. E. I. Schropp, H. A. Atwater, and A. Polman, "Improved red-response in thin film a-Si:H solar cells with soft-imprinted plasmonic back reflectors," Appl. Phys. Lett. **95**(18), 183503 (2009).
14. H. A. Atwater and A. Polman, "Plasmonics for improved photovoltaic devices," Nat. Mater. **9**(3), 205–213 (2010).
15. C. Rockstuhl, S. Fahr, and F. Lederer, "Absorption enhancement in solar cells by localized plasmon polaritons," J. Appl. Phys. **104**(12), 123102 (2008).

#184553 - $15.00 USD Received 31 Jan 2013; revised 23 Mar 2013; accepted 26 Mar 2013; published 2 Apr 2013

16. X.-H. Li, R. Song, Y.-K. Ee, P. Kumnorkaew, J. F. Gilchrist, and N. Tansu, "Light extraction efficiency and radiation patterns of III-nitride light-emitting diodes with colloidal microlens arrays with various aspect ratios," IEEE Photon. J. **3**(3), 489–499 (2011).
17. Y.-K. Ee, P. Kumnorkaew, R. A. Arif, H. Tong, J. F. Gilchrist, and N. Tansu, "Light extraction efficiency enhancement of InGaN quantum wells light-emitting diodes with polydimethylsiloxane concave microstructures," Opt. Express **17**(16), 13747–13757 (2009).
18. W. H. Koo, W. Youn, P. Zhu, X.-H. Li, N. Tansu, and F. So, "Light extraction of organic light emitting diodes by defective hexagonal-close-packed array," Adv. Funct. Mater. **22**(16), 3454–3459 (2012).
19. E. Matioli, E. Rangel, M. Iza, B. Fleury, N. Pfaff, J. Speck, E. Hu, and C. Weisbuch, "High extraction efficiency light-emitting diodes based on embedded air-gap photonic-crystals," Appl. Phys. Lett. **96**(3), 031108 (2010).
20. S. Fahr, C. Rockstuhl, and F. Lederer, "Engineering the randomness for enhanced absorption in solar cells," Appl. Phys. Lett. **92**(17), 171114 (2008).
21. R. A. Pala, J. White, E. Barnard, J. Liu, and M. L. Brongersma, "Design of plasmonic thin-film solar cells with broadband absorption enhancements," Adv. Mater. **21**(34), 3504–3509 (2009).
22. J. N. Munday and H. A. Atwater, "Large integrated absorption enhancement in plasmonic solar cells by combining metallic gratings and antireflection coatings," Nano Lett. **11**(6), 2195–2201 (2011).
23. P. Spinelli, M. Hebbink, R. de Waele, L. Black, F. Lenzmann, and A. Polman, "Optical impedance matching using coupled plasmonic nanoparticle arrays," Nano Lett. **11**(4), 1760–1765 (2011).
24. P. Spinelli, V. E. Ferry, J. van de Groep, M. van Lare, M. A. Verschuuren, R. E. I. Schropp, H. A. Atwater, and A. Polman, "Plasmonic light trapping in thin-film Si solar cells," J. Opt. **14**(2), 024002 (2012).
25. C. Rockstuhl, F. Lederer, T. Zentgraf, and H. Giessen, "Enhanced transmission of periodic, quasiperiodic, and random nanoaperture arrays," Appl. Phys. Lett. **91**(15), 151109 (2007).
26. V. E. Ferry, M. A. Verschuuren, M. C. Lare, R. E. I. Schropp, H. A. Atwater, and A. Polman, "Optimized spatial correlations for broadband light trapping nanopatterns in high efficiency ultrathin film a-Si:H solar cells," Nano Lett. **11**(10), 4239–4245 (2011).
27. Y. Nishijima, L. Rosa, and S. Juodkazis, "Surface plasmon resonances in periodic and random patterns of gold nano-disks for broadband light harvesting," Opt. Express **20**(10), 11466–11477 (2012).
28. P.-C. Tseng, M.-H. Hsu, M.-A. Tsai, C.-W. Chu, H.-C. Kuo, and P. Yu, "Enhanced omnidirectional photon coupling via quasi-periodic patterning of indium-tin-oxide for organic thin-film solar cells," Org. Electron. **12**(6), 886–890 (2011).
29. S. Linden, J. Kuhl, and H. Giessen, "Controlling the interaction between light and gold nanoparticles: Selective suppression of extinction," Phys. Rev. Lett. **86**(20), 4688–4691 (2001).
30. E. D. Palik, *Handbook of Optical Constants of Solids* (Academic, 1985).
31. A. Christ, "Optical properties of metallic photonic crystal structures," Ph.D. thesis, Philipps-Universität Marburg (2005).
32. C. Bauer, G. Kobiela, and H. Giessen, "2D quasiperiodic plasmonic crystals," Sci. Rep. **2**, 681 (2012).
33. S. Fan and J. D. Joannopoulos, "Analysis of guided resonances in photonic crystal slabs," Phys. Rev. B **65**(23), 235112 (2002).
34. M. J. Weber, *Handbook of Optical Materials* (CRC, 2003).
35. D. Zhou and R. Biswas, "Photonic crystal enhanced light-trapping in thin film solar cells," J. Appl. Phys. **103**(9), 093102 (2008).
36. C. Gueymard, "SMARTS2, Simple Model for the Atmospheric Radiative Transfer of Sunshine: Algorithms and performance assessment," Technical Report FSEC-PF-270–95, Florida Solar Energy Center, Cocoa, FL (1995).
37. J. G. Mutitu, S. Shi, C. Chen, T. Creazzo, A. Barnett, C. Honsberg, and D. W. Prather, "Thin film silicon solar cell design based on photonic crystal and diffractive grating structures," Opt. Express **16**(19), 15238–15248 (2008).
38. The latitude and longitude of Germany," *http://www.travelmath.com/country/Germany*. Accessed: 13/12/2012.
39. H. Schwarz and S. Ying, "Urban photovoltaic potential," in *2010 9th International Conference on Environment and Electrical Engineering (EEEIC)* (2010), pp. 26–28.

1. Introduction

Nowadays, renewable energies become more important due to the fact that several countries decided to phase out nuclear power and fossil fuels for security as well as for climate change reasons [1, 2]. Among the different kinds of renewable energies, solar energy has the potential to become one of the most used sources [3]. However, solar-grade silicon is expensive to produce [4]. Thus, the cost of solar cells requiring a large amount of silicon (Si) is also huge. In order to lower the costs of solar cells, the amount of Si has to be minimized, which can be achieved by reducing the Si layer thickness [4]. However, this results in a lower efficiency due to the weak absorption of visible light by Si [5]. In order to enhance the efficiency of thin-film solar cells, several approaches have been suggested. Most of the solar cell designs use an antireflection coating in order to minimize the amount of light reflected at the solar cell surface [6]. The efficiency can be further increased by using dye molecules [7–9]. Other possibilities of enhancing the efficiency of solar cells are the use of nanohole arrays [10], grating couplers [11], or plasmonic nanostructures [12–15]. The efficiency of LEDs,

#184553 - $15.00 USD Received 31 Jan 2013; revised 23 Mar 2013; accepted 26 Mar 2013; published 2 Apr 2013

which work in the opposite direction than solar cells, was also enhanced by using less ordered or quasicrystalline 2D grating structures [16–19]. Another approach is the use of a randomly textured Zinc oxide layer on top of the Si layer [20]. Whereas some of the solar cell designs are based on one-dimensional (1D) metallic photonic crystals [21, 22], others are making use of the periodic arrangement of metal structures in two dimensions (2D) [14, 23]. Spinelli et al. consider such 2D plasmonic structures on top of a thin-film c-Si layer [24]. Disordered [25–27] and quasiperiodic [25, 26, 28] structures have also been introduced. Whereas the quasiperiodic structures in the work of Ferry et al. [26] were mentioned only briefly, those in the paper of Tseng et al. [28] were discussed in detail. The latter paper covers different incident polar angles compared to an unpatterned solar cell. However, different azimuthal angles incident on the solar cell have not been examined, which is important together with the polar angle for the performance of the solar cell during the day as well as over the year. Moreover, no theoretical predictions have been provided in order to optimize the solar cell design. Here, we present predictions based on a Fano model for quasiperiodic plasmonic structures compared to periodic structures on top of a silicon-on-insulator solar cell design. We find that the enhancement factor for absorbed light in the quasicrystalline case is much less dependent on the azimuthal as well as the polar angle and is thus more constant during the day as well as over the year when compared to periodic structures.

2. Sample design

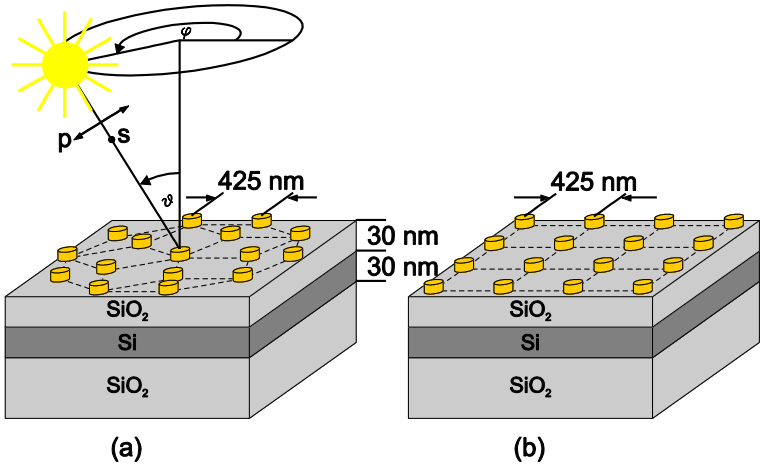

Fig. 1. Sample design with (a) a quasiperiodic arrangement as well as (b) a periodic arrangement of gold disks on top of a SiO_2/Si/SiO_2-substrate.

The sample structure is based on the metallic photonic crystal design of Linden et al. [29]. The sample substrate of our modelled structures consists of silicon dioxide (SiO_2) with a 30 nm thin crystalline silicon [30] layer on top. As a passivation layer serves SiO_2 of 30 nm thickness, which is located between the Si layer and a layer of gold disks. The gold disks with a diameter of 100 nm and a height of 50 nm are arranged in a quasiperiodic [on the vertices of an 8-5-approximant structure to the original Penrose tiling, see Fig. 1(a)] as well as in a periodic [see Fig. 1(b)] fashion in order to compare the individual enhancement factors. The edge length of the Penrose tiling [Fig. 1(a)] as well as the period of the square lattice [Fig. 1(b)] is 425nm. The passivation layer is needed in order to reduce the strong damping of the particle plasmon resonance, which takes place when a metal is directly placed on an absorbing semiconductor [21]. Additionally, the more symmetric layer structure shifts the cutoff energy of waves that can be guided in the Si layer to lower values [31].

#184553 - $15.00 USD Received 31 Jan 2013; revised 23 Mar 2013; accepted 26 Mar 2013; published 2 Apr 2013

3. Results and discussion

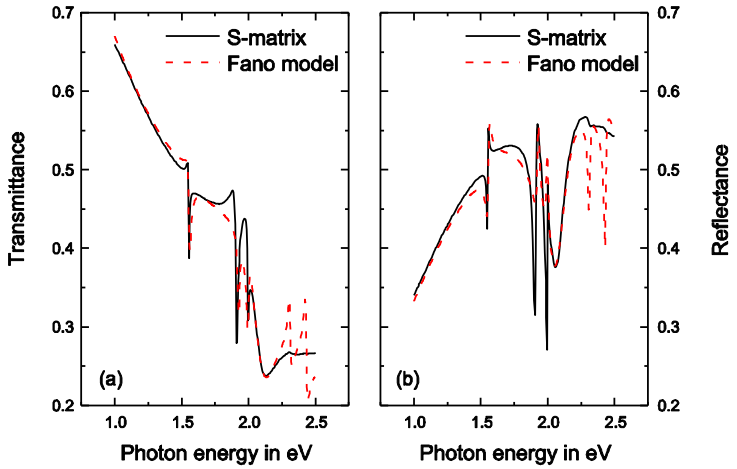

Fig. 2. S-matrix calculated (a) transmittance and (b) reflectance spectra (black solid lines) as well as the corresponding Fano modelled spectra (red dashed lines) for a periodic gold disk arrangement.

The predictions in this paper are based on the simulation model presented in [32]. In order to use reasonable fitting parameters, the normal incidence spectra for the periodic gold disk arrangement are simulated by using Scattering matrix (S-matrix) calculations. The transmittance and reflectance spectra are shown as black solid curves in Figs. 2(a) and 2(b), respectively. The broader resonance in the energy range between 2 eV and 2.25 eV corresponds to a particle plasmon resonance, whereas the sharp resonances at about 1.5 eV, 1.9 eV, and 2 eV stem from waves that are coupled into the Si layer due to the grating structure. In order to be able to model the optical properties of a metallic photonic quasicrystal, a Fano model [33] for the transmitted and reflected light has to be used. The transmission and reflection amplitudes *t* and *r* in this model are

$$t = t_d \exp(i\phi_t) - t_{Pl} \frac{\Gamma_{Pl} \exp(i\phi_{Pl})}{E - E_{Pl} + i\Gamma_{Pl}} - C\sum_k t_k \frac{\Gamma_k \exp(i\phi_k)}{E - E_k + i\Gamma_k}, \quad (1)$$

$$r = r_d \exp(i\phi_r) + r_{Pl} \frac{\Gamma_{Pl} \exp(i\phi_{Pl})}{E - E_{Pl} + i\Gamma_{Pl}} + C\sum_k r_k \frac{\Gamma_k \exp(i\phi_k)}{E - E_k + i\Gamma_k} \quad (2)$$

with the direct transmission and reflection coefficients

$$t_d = 1.3370 - 0.8147E + 0.3420E^2 - 0.0575E^3, \quad (3)$$

$$r_d = 0.0325 + 0.7545E - 0.2046E^2 + 0.0053E^3. \quad (4)$$

t_d and r_d are fitted to the transmittance and reflectance spectra of the structure without the plasmonic dots, respectively. The corresponding phases are given by $\phi_t = 0.269\pi$ and $\phi_r = 0.864\pi$. The spectral width, the phase, and the energy of the particle plasmon resonance are set to $\Gamma_{Pl} = 0.1081\,\text{eV}$, $\phi_{Pl} = \frac{\pi}{2}$, and $E_{Pl} = 2.0722\,\text{eV}$. The sum over all waveguide

#184553 - $15.00 USD Received 31 Jan 2013; revised 23 Mar 2013; accepted 26 Mar 2013; published 2 Apr 2013

modes present in the energy range E is dependent on the spectral widths $\Gamma_k = 0.01\,\mathrm{eV}$, the amplitudes $t_k = r_k$, the energies E_k, and the phases ϕ_k. Details of how to obtain the different amplitudes, energies, and phases can be found in [32]. However, the phases of the undisturbed waveguide modes are given by $\phi_{t,\infty} = 0.4104\pi$ and $\phi_{r,\infty} = 0.7096\pi$. The fitting parameters in order to obtain the correct ratio between particle plasmon and waveguide modes are t_{Pl} = 0.1512, r_{Pl} = 0.1668, and C = 0.01025. With these parameters the transmittance and reflectance spectra are modelled, which are shown as red dashed curves in Figs. 2(a) and 2(b), respectively. The agreement between the S-matrix simulations and the Fano model is quite good. Note that the waveguide modes in the S-matrix spectra above 2.2 eV are damped due to the increased absorption coefficient of the silicon layer in this energy range. This is neglected in the Fano model. However, due to the fact that the waveguide modes cannot be excited above 2.2 eV, the absorption above this value should be about the same for both structural arrangements. Therefore, the spectra in the following are only considered in the energy region below this value. Moreover, an electron-hole pair in silicon can only be excited above the band gap energy E_g = 1.12 eV [34]. Therefore, only energies above this value are utilized.

The important property for solar cells is the absorbance A of light instead of the reflectance R and the transmittance T. It can be calculated by using $A = 1 - R - T$. All reflectance and transmittance spectra are calculated by using the parameters given above. It can be assumed that each photon absorbed in the Si layer is able to create an electron-hole pair [22]. However, the absorbance calculated above also includes the part of the light that is absorbed in the gold disks. This is in the energy region where the particle plasmon is excited. Therefore, the absorbance in the silicon layer is lower than calculated in the following. However, the amount of absorbed light in the gold disks is expected to be independent of their structural arrangement, thus being equal for the Penrose tiling and the square lattice. Moreover, the excited waveguide modes are mostly concentrated within the silicon layer and thus being primarily absorbed therein.

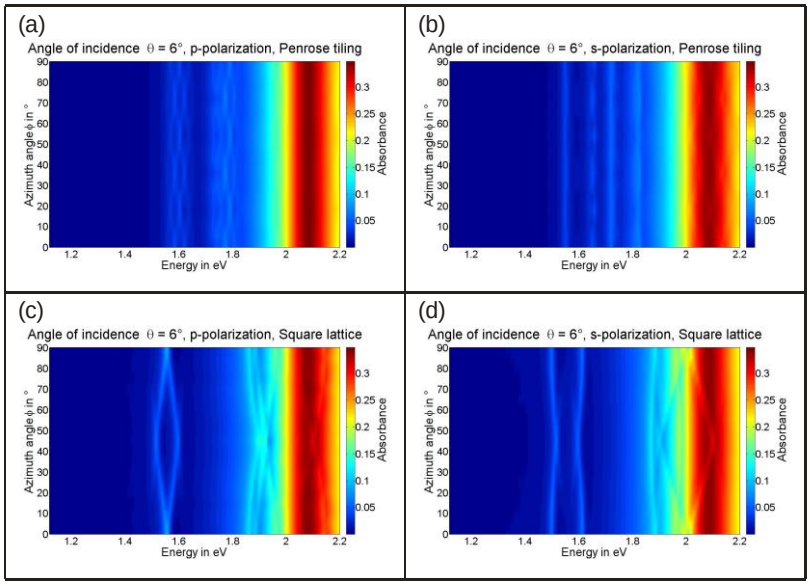

Fig. 3. Polarization dependent absorbance spectra for (a) p- and (b) s-polarized light of a Penrose tiling as well as (c) p- and (d) s-polarized light of a square lattice for an angle of incidence θ = 6°. The azimuthal angle ϕ was changed between 0° and 90°.

Since the angle of incidence as well as the azimuthal angle of sunlight incident on a fix-mounted non-tracking solar cell change during the course of the day as well as the year, the

#184553 - $15.00 USD Received 31 Jan 2013; revised 23 Mar 2013; accepted 26 Mar 2013; published 2 Apr 2013

angle dependent and the polarization dependent absorbance spectra have to be considered. First, we have a look at the absorbance spectra dependent on the incident azimuthal angle [see Fig. 3]. The p- and s-polarized absorbance spectra for a Penrose tiling at an incidence angle of 6° are displayed in Figs. 3(a) and 3(b), where the azimuthal angle is changed between 0° and 90° in the energy range of 1.12 eV and 2.2 eV. The absorbance is color coded in these plots. As comparison, the polarization dependent absorbance spectra in p- and s-polarization for a square lattice are shown in Figs. 3(c) and 3(d), respectively. One can recognize that the absorbance maxima of the quasiperiodic structure stay at approximately the same energy position, which is almost independent of the incident azimuthal angle. For the periodic arrangement, however, these absorbance maxima strongly depend on the incident azimuthal angle. This is even worse for larger polar angles. Therefore, the absorbance spectra of the Penrose tiling are much less polarization dependent and thus more isotropic than those of the square lattice due to the higher rotational symmetry of the quasicrystal. This means that almost the same absorbance is expected for the quasiperiodic arrangement for any incident azimuthal angle. This is desirable since the incident azimuthal angle varies for different times during the day as well as the year.

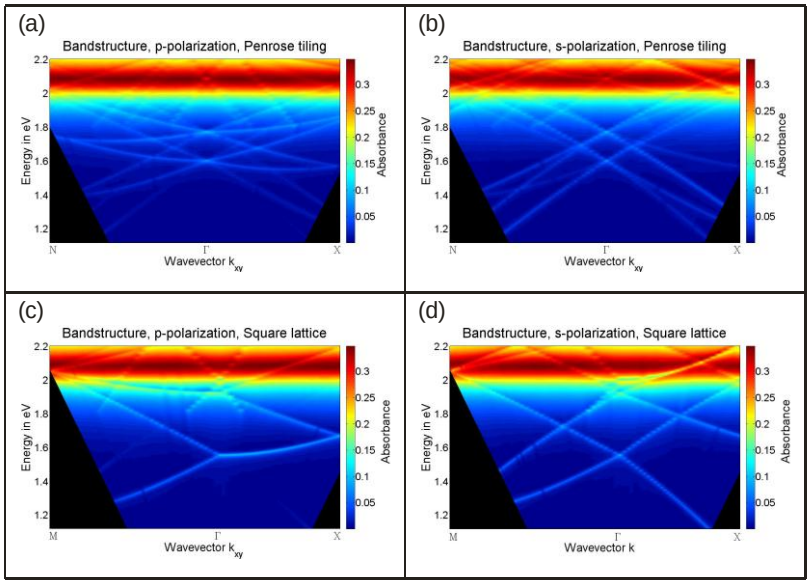

Fig. 4. Angle dependent absorbance spectra for (a) p- and (b) s-polarized light of a Penrose tiling as well as (c) p- and (d) s-polarized light of a square lattice. The part from Γ to N belongs to an azimuthal angle of 18° and the part from Γ to M to $\phi = 45°$. The part from Γ to X belongs to an azimuthal angle of 0°.

For the other important parameter, namely the angle of incidence, the angle dependent absorbance spectra were calculated, which is shown in Fig. 4 for a quasiperiodic [Figs. 4(a) and 4(b)] as well as for a periodic gold disk arrangement [Figs. 4(c) and 4(d)] in p- as well as in s-polarization. Normal incidence is denoted as Γ and the (pseudo-)Brillouin zone edge for an azimuthal angle of 0° is denoted as X [see right part in Figs. 4(a) – 4(d)]. The pseudo-Brillouin zone edge of the Penrose tiling with an azimuthal angle of 18° is marked as N, whereas the Brillouin zone edge of the square lattice with an azimuthal angle of 45° is described by M [see left part in Figs. 4(a)–4(d)]. For the structure with the quasicrystalline lattice much more waveguide modes are visible compared to the periodic lattice. The spectral range for the Penrose tiling is much better covered than for the square lattice. Additionally, the spectra in directions X and N for the Penrose tiling are much more similar to each other than those in directions X and M for the periodic structure.

#184553 - $15.00 USD Received 31 Jan 2013; revised 23 Mar 2013; accepted 26 Mar 2013; published 2 Apr 2013

Since the angle of incidence as well as the azimuthal angle on a solar cell changes during the day as well as over the year, the efficiency should not vary much with θ and ϕ. Therefore, the average absorption A_{avg} is calculated by using [35]

$$A_{avg} = \int_{\lambda_{min}}^{\lambda_g} A_{tot}(\lambda)\, S(\lambda)\, \mathrm{d}\lambda \tag{5}$$

with $S(\lambda)$ as the direct solar and circumsolar spectrum, $\lambda_{min} = 1240/E_{max}$, and $\lambda_g = 1240/E_g$. The values for E_g and E_{max} are the above mentioned 1.12 eV and 2.2 eV, respectively. The total absorption $A_{tot}(\lambda)$ of Eq. (5) is obtained by averaging over the p- and s-polarized absorbance spectra $A_{p\text{-}pol}$ and $A_{s\text{-}pol}$:

$$A_{tot}(\lambda) = \frac{A_{p-pol}(\lambda) + A_{s-pol}(\lambda)}{2}. \tag{6}$$

Since $S(\lambda)$ is dependent on the air mass the sunlight is propagating through, $S(\lambda)$ varies for different zenith angles of the sun and thus also for different incidence angles. The different air mass irradiance spectra are calculated by using the *Simple Model for the Atmospheric Radiative Transfer of Sunshine* (SMARTS2) [36]. The enhancement factor EF is obtained by normalizing the average absorption of the enhanced structure $A_{avg,enh}$ by that of the bare substrate $A_{avg,Bare}$ [37]

$$EF = \frac{A_{avg,enh}}{A_{avg,Bare}}, \tag{7}$$

where the enhanced structure is either the structure with the quasiperiodic ($A_{avg,Penrose}$) or the periodic ($A_{avg,Square}$) gold disk arrangement. The bare substrate has exactly the same sample design than the enhanced structures but without the metal disks on top. In order to obtain $A_{avg,Bare}$, the S-matrix calculated absorbance spectra of the bare substrate are used in Eq. (6).

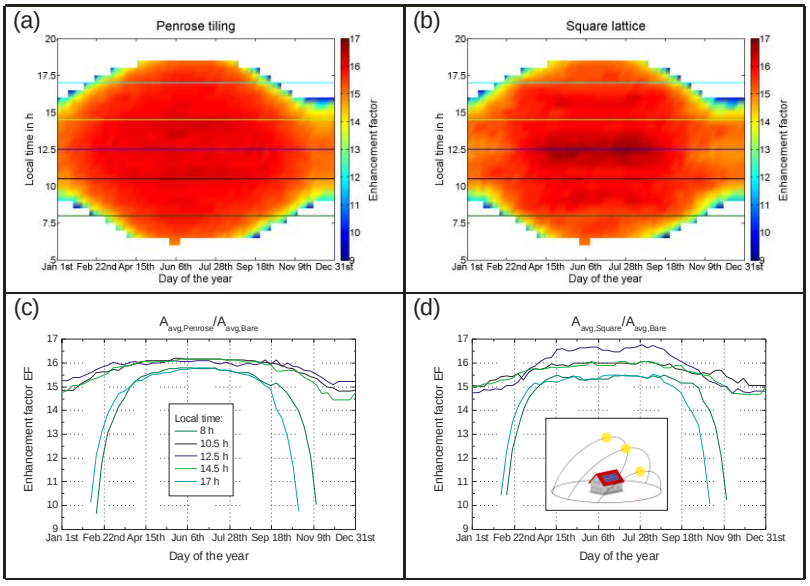

Fig. 5. Enhancement factor versus day of the year and local time for (a) a Penrose tiling as well as for (b) a square lattice. The colored lines in (a) and (b) show the cross sections of the enhancement factor for specific local times, which is plotted versus the day of the year for (c) a Penrose tiling and (d) a square lattice. The inset in (d) shows the course of the sun for three different days of the year.

#184553 - $15.00 USD Received 31 Jan 2013; revised 23 Mar 2013; accepted 26 Mar 2013; published 2 Apr 2013

Since the angle of incidence on the solar cell is dependent on the day of the year as well as the local time of the day, it is more convenient to plot the color coded enhancement factor versus the day of the year and the local time as shown in Figs. 5(a) and 5(b). These Figs. are calculated by assuming an average latitude and longitude of Germany, which is approximately 51° N and 9° E [38], and by assuming an average roof pitch of 35° [39] with a solar cell directing to the south. The course of the sun in such a case is shown in the inset of Fig. 5(d) for three different times of the year. The upper ellipse shows the course of the sun in summer, whereas the central and lower ones belong to spring/fall and winter, respectively. Sunrise is always in the back of the Fig. and sunset in the front.

In Figs. 5(a) and 5(b), one can see that the enhancement factor of the Penrose tiling [Fig. 5(a)] is much more constant during the day as well as over the year when compared to the enhancement factor of the square lattice [Fig. 5(b)]. This is even true in the morning hours and the late afternoons during summer [see bottom and top of Figs. 5(a) and 5(b)] as well as during the whole year for local times around noon. The cross sections for local times of 8 a.m., 10:30 a.m., 12:30 p.m., 2:30 p.m., and 5 p.m. are shown as dark green, black, blue, light green, and cyan solid curves in Figs. 5(a) and 5(b). These cross sections are plotted versus the day of the year in the corresponding colors in Figs. 5(c) and 5(d) for a Penrose tiling and a square lattice, respectively. The curves for the Penrose tiling and the square lattice at 10:30 a.m. and 2:30 p.m. show in principle similar enhancement factors with a value of about 15 during winter-time and a value of about 16 during summertime. However, the enhancement factor of the quasiperiodic structure rises slightly faster and shows a nearly constant value between 15.8 and 16.2 from the beginning of March to the mid of October, whereas the enhancement factor of the periodic structure varies between 15.5 and 16.1 during the same period of time. Only between the beginning of April and the mid of September the enhancement factor of the periodic lattice is in the same region than that of the Penrose tiling.

The structure with the quasiperiodic arrangement for a local time around noon also shows essentially the behavior as for local times at 10:30 a.m. and 2:30 p.m., but with a slightly bigger enhancement factor in wintertime. In contrast, the structure with the square lattice around noon is increased during summertime to a value of about 16.6, but it is also decreased to a value of about 14.7 during wintertime. Moreover, the enhancement factor stays longer at values around 15 when compared to the quasicrystalline lattice. However, it is desirable to reach the same enhancement factors throughout the whole year and the whole day, which is reached better in the quasicrystalline case. Especially in the morning and evening hours a relatively high value is preferable since more energy is needed during these hours. Nevertheless, the enhancement factors in the morning as well as in the late afternoon are decreased for both structural arrangements. However, the maximum enhancement factor for the Penrose tiling reaches a value of about 15.8, whereas that of the square lattice has only a value of about 15.5. Only in wintertime in the morning and the late afternoon, the enhancement factor is much lower for both structural arrangements due to the huge zenith angle.

In summary, the enhancement factors during summertime range between 15.8 and 16.2 for the Penrose tiling as well as between 15.4 and 16.6 for the square lattice. Moreover, for local times between 10 a.m. and 3 p.m., the enhancement factor during wintertime drops to a value of below 15 for the square lattice and stays at values around 15 for a quite long period of time, whereas the enhancement factor during that local time increases much faster and stays most of the year at values between 15.8 and 16.2 for the Penrose tiling. Additionally, the enhancement factor during summertime of the quasiperiodic lattice is larger in the morning and the afternoon when compared to the periodic case. This indicates that the enhancement factor is much more constant in the quasicrystalline case, leading to a more constant performance of the solar cell during the day as well as over the year.

Furthermore, it is possible to integrate the average absorption over the local time t_{LT} as well as the day of the year t_{day} and to normalize the enhanced structure to the bare structure. By doing so, a value of EF_{tot} = 15.573 is obtained for the quasicrystalline structure as well as a value of EF_{tot} = 15.515 for the periodic structure with

#184553 - $15.00 USD Received 31 Jan 2013; revised 23 Mar 2013; accepted 26 Mar 2013; published 2 Apr 2013

$$EF_{tot} = \frac{\int_1^{365}\int_0^{24} A_{avg,enh}\ \mathrm{d}t_{LT}\ \mathrm{d}t_{day}}{\int_1^{365}\int_0^{24} A_{avg,Bare}\ \mathrm{d}t_{LT}\ \mathrm{d}t_{day}}. \quad (8)$$

This means that even the total enhancement factor EF_{tot} is slightly increased for the Penrose tiling. Even though the enhancement factor for the square lattice reaches a value of 16.6 around noon during summer, the total enhancement factor of the Penrose tiling is slightly larger due to the more constant values during the course of the day as well as over the year.

4. Conclusion

We have calculated the absorbance spectra for different polar and azimuthal angles for thin-film silicon solar cells. Absorption enhancement compared to the bare silicon-on-insulator substrate was reached by introducing a layer of gold disks placed on top of the Si layer in a 2D quasiperiodic as well as a 2D periodic fashion. The calculated absorbance spectra are based on a Fano model with fitting parameters obtained from fits to the normal incidence S-matrix simulations. We have shown that the structure with the Penrose tiling is much more isotropic than that with the square lattice and also excites much more waveguide modes for absorbance spectra dependent on the azimuthal angle as well as the angle of incidence. This leads to a more constant enhancement factor throughout the day as well as over the year. The variation during summertime ranges between 15.8 and 16.2 for the quasiperiodic lattice, even in the morning and evening hours, whereas the value changes between 15.4 and 16.6 for the periodic lattice. In the quasicrystalline case, this range is valid between the beginning of March and the mid of October, at least for local times between 10:30 a.m. and 2:30 p.m. In contrast, the enhancement factor varies for the square lattice during the same period of time between 15.5 and 16.6. Additionally, the total enhancement factor is slightly larger for the quasiperiodic lattice. Therefore, the performance of the solar cell with a quasicrystalline arrangement is expected to be more stable than that with a periodic arrangement. In particular, during morning and evening hours the Penrose lattice provides higher enhancement. This is desirable as energy consumption is highest at that time. Also, a more evenly distributed solar power feed is beneficial for the stability of the electric grid. The purpose of this paper was to predict the absorption enhancement of a quasiperiodic compared to a periodic solar cell. However, the design of the solar cell can still be optimized and the predictions should be verified by experiments, what has to be done for future research. A higher density of the plasmonic disks, i.e., a smaller period, shifts all waveguide modes to higher energies. In a thicker Si layer more waveguide modes are expected for both structural arrangements.

Acknowledgments

The authors thank S. Hein for help with graphical visualizations. This work was financially supported by Deutsche Forschungsgemeinschaft (Open Access Publishing, SPP1391, and FOR557), by Baden-Württemberg Stiftung, and by BMBF (13N9155 and 13N10146).

#184553 - $15.00 USD Received 31 Jan 2013; revised 23 Mar 2013; accepted 26 Mar 2013; published 2 Apr 2013